THE JOURNAL OF PHYSICAL CHEMISTRY LETTERS
A JOURNAL OF THE AMERICAN CHEMICAL SOCIETY

pubs.acs.org/JPCL Letter

Long-Range Nonequilibrium Coherent Tunneling Induced by Fractional Vibronic Resonances

R. Kevin Kessing,* Pei-Yun Yang,* Salvatore R. Manmana,* and Jianshu Cao*

Cite This: *J. Phys. Chem. Lett.* 2022, 13, 6831−6838 Read Online

ACCESS | Metrics & More | Article Recommendations | Supporting Information

ABSTRACT: We study the influence of a linear energy bias on a nonequilibrium excitation on a chain of molecules coupled to local vibrations (a tilted Holstein model) using both a random-walk rate kernel theory and a nonperturbative, massively parallelized adaptive-basis algorithm. We uncover structured and discrete vibronic resonance behavior fundamentally different from both linear response theory and homogeneous polaron dynamics. Remarkably, resonance between the phonon energy $\hbar\omega$ and the bias δ_ϵ occurs not only at integer but also fractional ratios $\delta_\epsilon/(\hbar\omega) = m/n$, which effect long-range n-bond m-phonon tunneling. These observations are reproduced in a model calculation of a recently demonstrated Cy3 system, and the effect of dipole−dipole-type non-nearest-neighbor coupling and vibrationally relaxed initial states is also considered. Potential applications range from molecular electronics to optical lattices and artificial light harvesting via vibronic engineering of coherent quantum transport.

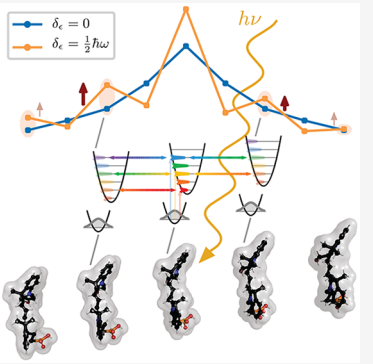

The quantum dynamics of charge carriers and excitations in molecular systems is of great significance to a variety of research areas ranging from physics to material science, chemistry, and biology. Molecular vibrational degrees of freedom, which are quantized into phonons, can strongly influence such dynamics.[1] The Holstein model is a prototypical model for such electron−phonon (vibronic) coupling and has been widely applied to various systems including polymers, molecular aggregates, and semiconductors.[2−10] A further crucial ingredient to such dynamics is an energy gradient or "tilt" representing, for example, a voltage gradient in measurements of charge mobility or a natural energy funnel.[11−14] Such biased vibronic systems exhibit various important coherent electron−phonon transport effects which have recently attracted much attention,[15,16] such as "phonon-assisted resonant tunneling" in inelastic tunneling experiments[17−19] or the "Franck−Condon (FC) blockade" in quantum dot or molecular tunneling experiments,[20,21] as well as vibrational enhancement of transport in antenna protein complexes.[5,13,22−24] On the other end, initial experimental evidence of vibronic resonance may reach back to 1970[25] (though not without controversy[26]). However, theoretical treatments of these phenomena have used perturbative approaches[12] to calculate steady-state currents through one[20] or two[16] sites, were limited to the linear-response regime[27] or single-phonon transitions,[28] or considered equilibrium initial states.[29]

In this paper, we report striking higher-order *fractional* and *long-range* resonances that occur within the "forbidden" FC blockaded regime when multiple sites are concatenated and their full nonequilibrium dynamics calculated nonperturbatively. Previously, phononless long-range resonant tunneling has been studied theoretically and experimentally in cold-gas quantum simulators on tilted optical lattices,[30−39] and such setups have been employed to investigate a plethora of phenomena such as quantum magnetism,[30,33,38,39] quantum dimer models,[32] transport properties and dynamical phase transition points,[34,35,40] or the creation of anyons.[41] We show that vibronic coupling naturally realizes and generalizes such resonant tunneling behavior.

MODEL

Figure 1a illustrates our setup: a chain of L linearly tilted molecular sites which interact via nearest-neighbor coupling J and couple linearly to local vibrations. These vibrational degrees of freedom are represented by a single dominant mode, assumed to be harmonic with frequency ω, and each molecular site is coupled strongly to its own vibrational mode. The coupling to the vibrations is quantified by the parameter g, related to the Huang−Rhys parameter as $S = \left(\frac{g}{\hbar\omega}\right)^2$. A linear tilt shifts the energy of each site j relative to site $j-1$ by δ_ϵ. The resulting Hamiltonian is

$$H = \sum_{j=0}^{L-1} \left[J(|j\rangle\langle j+1| + \text{h.c.}) + \hbar\omega\left(b_j^\dagger b_j + \frac{1}{2}\right) + g n_j^{\text{exc}}(b_j + b_j^\dagger) + \delta_\epsilon j n_j^{\text{exc}} \right] \quad (1)$$

Received: May 13, 2022
Accepted: July 12, 2022

https://doi.org/10.1021/acs.jpclett.2c01455
J. Phys. Chem. Lett. 2022, 13, 6831−6838

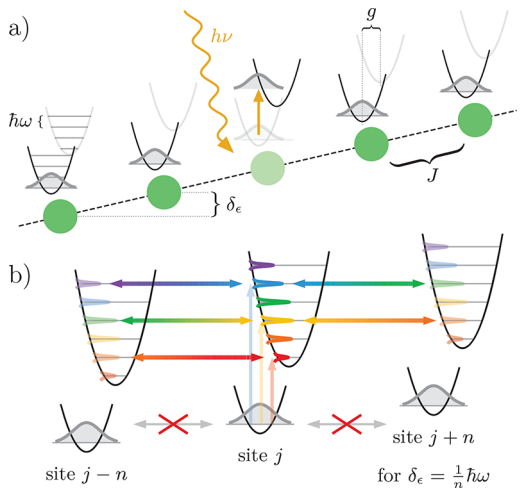

Figure 1. (a) Sketch of the system: On the central site, a Franck–Condon (FC) excitation is induced, which tunnels to neighboring sites with amplitude J and interacts with local phonons $\hbar\omega$ via Holstein coupling g in the presence of a linear potential bias δ_ϵ. (b) Resonant transitions are possible between local eigenstates of the excited PES. The FC excitation is a superposition of many different local eigenstates, allowing for multiple resonant vibronic transitions to both sides.

where $|j\rangle$ is the excitonic state localized on site j (where $\langle i|j\rangle = \delta_{ij}$); $n_j^{\mathrm{exc}} = |j\rangle\langle j|$ is the number of excitons on this site (restricted to 0 or 1); b_j ($b_j^\dagger$) is the bosonic annihilation (creation) operators for phonons at site j; and $\hbar\omega(b_j^\dagger b_j + {}^1/_2)$ is the local harmonic vibrational Hamiltonian on site j. To accommodate the strong vibronic coupling, we truncate the vibrational Hilbert spaces at $\nu_{\max} = 127$ phonons per mode, following ref 42. We investigate the dynamics of a single Franck–Condon (vertical) excitation from the vibrational and electronic ground state, which is initially (time $t = 0$) localized to the central site. In every calculation, boundary effects are minimized by using a sufficiently large chain length L such that the exciton population at the boundary is always less than 0.7% (with the exception of Figure 4a,b, where the excitation is placed at the rightmost edge for visualization purposes).

The model allows for multiple interpretations in different contexts: $|j\rangle$ can represent the first excited state at the jth molecule with electronic ground states on the remaining molecules. However, $|j\rangle$ can also stand for a charged state arising from injecting an electron into the jth molecular site, or for an atom placed at a certain position in an optical lattice, lending the findings possible relevance in various situations such as light harvesting, cold gas optical lattices, organic semiconductors, or nonequilibrium molecular junctions.

NUMERICAL METHOD

To present a complete dynamical picture, we have developed both a numerical algorithm and an analytical approach. Our massively parallelized numerical method is based on dynamically adapted effective basis sets, which can be grouped to the expanding family of adaptive basis methods (cf., refs 43–52; see SI for details) but is technically most similar to a repeated dynamic use of "limited functional spaces"[53,54] (see also refs 55 and 29), and which can be applied in principle to arbitrary quantum dynamics problems. By exploiting Hilbert-space localization of physically relevant states, the method computes dynamics only in the most relevant subspace, which is adaptively reconfigured to follow the evolving wave function. The parallel nature of the linear-algebra problem is further leveraged by optimizing the method to be run on graphics processing units (GPUs), granting a substantial boost in runtime efficiency over existing methods, while still allowing treatment of both large local dimensions (up to $\nu_{\max} = 255$) or large chain lengths (up to $L = 301$) (see the Supporting Information (SI) for further details). To verify several important features of these numerical findings, we develop a random walk model with transition probabilities obtained from perturbation theory and evaluated using path integrals, as described below.

RESONANCE-ENHANCED TRANSPORT AND MULTIMODAL STATES

We first calculate the Holstein dynamics for a range of values of the tilt parameter δ_ϵ and two different (J-aggregate-like)

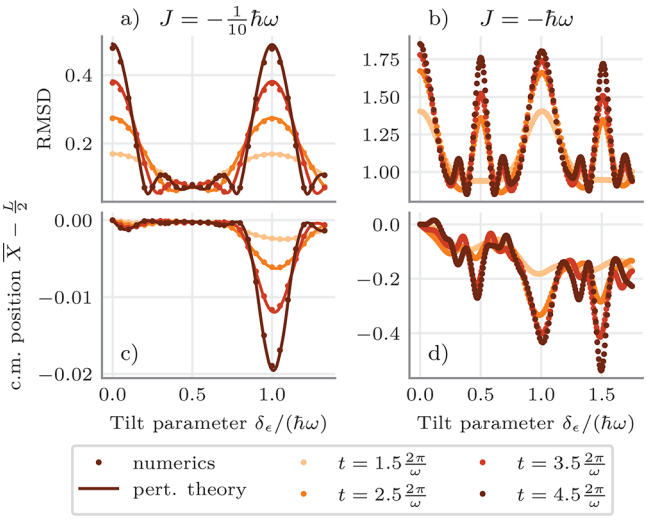

Figure 2. Excitonic RMSD and movement of the average exciton position in a tilted Holstein chain for a series of tilt parameter values δ_ϵ after different times t: (a,c) perturbation theory (lines) and numerics (dots) for weak hopping $J = -\frac{1}{10}\hbar\omega$ with $L = 9$; (b,d) numerical data for strong hopping $J = -\hbar\omega$ with $L = 19$. For all data: $g = 4\hbar\omega$ (strong vibronic coupling).

values of J. In Figure 2, the average position of the particle, $\bar{X} := \sum_{j=0}^{L-1} j\,\langle n_j^{\mathrm{exc}}\rangle$, and its root-mean-square deviation (RMSD),

$$\mathrm{RMSD} = \sqrt{\sigma^2} := \sqrt{\sum_{j=0}^{L-1} \langle n_j^{\mathrm{exc}}\rangle [j - \bar{X}]^2}$$

are plotted as a function of the tilt parameter δ_ϵ at different times. Interestingly, the RMSD as a function of δ_ϵ is highly nonlinear, exhibiting strong spikes around integer and half-integer values of $\delta_\epsilon/(\hbar\omega)$. Additionally, smaller spikes appear around $\delta_\epsilon/(\hbar\omega) \in \{{}^1/_3, {}^2/_3, {}^4/_3\}$. Between these values, propagation is strongly suppressed, suggesting transport-enhancing resonances are realized at certain values of δ_ϵ. Varying the remaining Hamiltonian parameters reveals that the location of the maxima depends only on the ratio $\delta_\epsilon/(\hbar\omega)$ (see SI section 2). Note that the observed resonances for $|\delta_\epsilon| < \hbar\omega$ lie within the "forbidden" FC blockade regime.[20]

https://doi.org/10.1021/acs.jpclett.2c01455
J. Phys. Chem. Lett. 2022, 13, 6831−6838

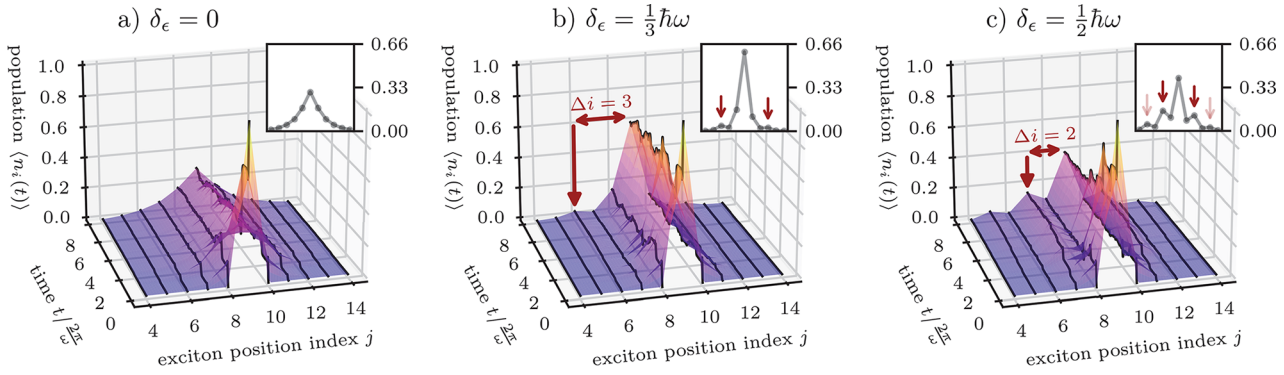

Figure 3. Spatial exciton distribution over time with $J = -\hbar\omega$ (as shown in Figure 2b,d) for the (a) homogeneous ($\delta_\epsilon = 0$), (b) third-order resonant ($\delta_\epsilon = 1/3\hbar\omega$), and (c) second-order resonant ($\delta_\epsilon = 1/2\hbar\omega$) cases. The insets show the exciton distribution at the final time $t = 8\frac{2\pi}{\omega}$. In the second- and third-order resonant tilted cases, the exciton does not simply propagate outward from a central peak into smooth tails, but instead excitonic density peaks form at the resonant sites, located n sites from the initial site for $\delta_\epsilon = 1/n\hbar\omega$.

Furthermore, Figure 3 shows that the dynamics of the local density in the tilted chains behaves completely differently than in an untilted chain. For $\delta_\epsilon = 0$, the exciton propagates into a symmetric, peaked state that extends over a few lattice states, as shown in Figure 3a (cf., ref 42). However, if δ_ϵ is set to a resonant value, the final state is no longer a single-peak state, but exhibits multiple peaks and dips in its local exciton distribution. Further numerical results (see SI section 3) explicitly show that the density n sites off-center is maximized when δ_ϵ is a multiple of $1/n\hbar\omega$.

This brings us to our main insight: When the parameters are resonant as $\delta_\epsilon/(\hbar\omega) = m/n$ where n and m are small integers, then an excitation that is initially localized at site j will tunnel to sites $j \pm n$ (and from there to sites $j \pm 2n$, etc.). In other words, the nearest-neighbor tunneling behavior of an unbiased chain is replaced by phonon-mediated (vibronic) tunneling over n sites, leading to spatially structured, multimodal states—or effectively suppressing the tunneling if n is too large or $\delta_\epsilon/(\hbar\omega) \notin \mathbb{Q}$. This n-site tunneling is the origin of the RMSD spikes seen in Figure 2. We note that though arbitrary integers m and n fulfilling $m/n = \delta_\epsilon/(\hbar\omega)$ will (in principle) produce resonances, finite J will limit observable tunneling for large n. Furthermore, large m decreases the number of resonant $|\nu'\rangle$ states in the uphill direction, limiting transport.

Remarkably, certain resonant shifts δ_ϵ strongly promote diffusivity, for example, $\delta_\epsilon = \frac{\hbar\omega}{2}$ in Figure 2. In the case of strong vibronic coupling, propagation is then enhanced in both the "uphill" *and* "downhill" direction—that is, the direction of increasing (to the right) and decreasing potential (left), respectively—even for iterated resonant tunneling processes ($j \to j \pm 2 \to j \pm 4$), which might be exploited experimentally to engineer vibronically optimized transport.

THE RESONANCE MECHANISM

The observed resonant tunneling is due to matching energies between vibronic states at different sites, as illustrated in Figure 1. Denoting the excited-state PES vibrational eigenstates as $|\nu'\rangle$ and those of the ground state PES as $|\nu\rangle$, we find that the Franck–Condon $|\nu = 0\rangle$ state is a g-dependent superposition of many different $|\nu'\rangle$ eigenstates, given by the coherent state formula[56] $|\nu = 0\rangle \propto \sum_{\nu'} \frac{\alpha^{\nu'}}{\sqrt{\nu'!}}|\nu'\rangle$ with $\alpha = \frac{g}{\hbar\omega}$. Then, if $\delta_\epsilon = \hbar\omega$, every constituent $|\nu'\rangle$ state of a Franck–Condon state is isoenergetic with the state $|\nu' + 1\rangle$ at the downhill neighboring site and $|\nu' - 1\rangle$ at the uphill neighbor, opening up multiple resonant transition pathways. More generally, for $\delta_\epsilon = m/n\hbar\omega$, the resonant transitions are mediated by m-phonon and n-fold hopping matrix elements. Further, once the particle has tunneled from a state $|\nu'\rangle$ at site j to $|\nu' \pm m\rangle$ at site $j \pm n$, the process can be successively repeated, tunneling to sites $|\nu' \pm 2m\rangle$ at $j \pm 2n$, etc. Interestingly, if the initial state is localized to a single site, then the exciton dynamics are completely independent of the sign of J. This can be understood by considering the spatially localized state in the delocalized-exciton eigenbasis, where it experiences at most a global phase change under $J \mapsto -J$ (see SI section 4).

We can compare this behavior to the dynamics of a tilted Bose–Hubbard chain in the Mott insulating phase $|J \ll |U|$ with equal filling n_0 at each site.[30,33,37] When the tilt constant δ_ϵ is a simple fraction of the Hubbard interaction, $\delta_\epsilon = U/n$, a single boson can tunnel from any site in the downhill direction by n sites to form a state that is isoenergetic with the initial state.[37,39] The resonant states can be mapped to dipoles and can be used to construct effective spin or quantum dimer models.[30,32,39] The resonant tunneling we observe in the tilted Holstein model is similar to that in tilted Bose-Hubbard systems, but differs in some key aspects: (i) The multiple excited $|\nu'\rangle$ states that constitute the Franck–Condon excitation allow for tunneling in both the downhill *and* uphill direction, whereas the Mott insulating state only allows for downhill transitions. (ii) Our localized initial state induces tunneling from a single site. (iii) Most importantly, the equidistant spacing of the vibrational QHO levels means that a repeated tunneling process is possible, since each tunneling event is energetically equivalent to an iterated tunneling, giving rise to the secondary resonance peaks in Figure 3c and Figure 4b. In contrast, in the Hubbard model, a doublon is bound to the first resonant site.[30]

RANDOM-WALK RATE KERNEL MODEL

To further support our findings, we verify the numerical results using an analytic approach based on hopping-rate kernels, which does not invoke the Markov approximation as in previous studies[57,58] and therefore belongs to the growing number of non-Markovian methods for open quantum systems (e.g., the transfer tensor method[59]). The resulting kinetics is equivalent to a continuous-time random walk, that is, a generalization of Poisson kinetics on networks.[60,61]

https://doi.org/10.1021/acs.jpclett.2c01455
J. Phys. Chem. Lett. 2022, 13, 6831–6838

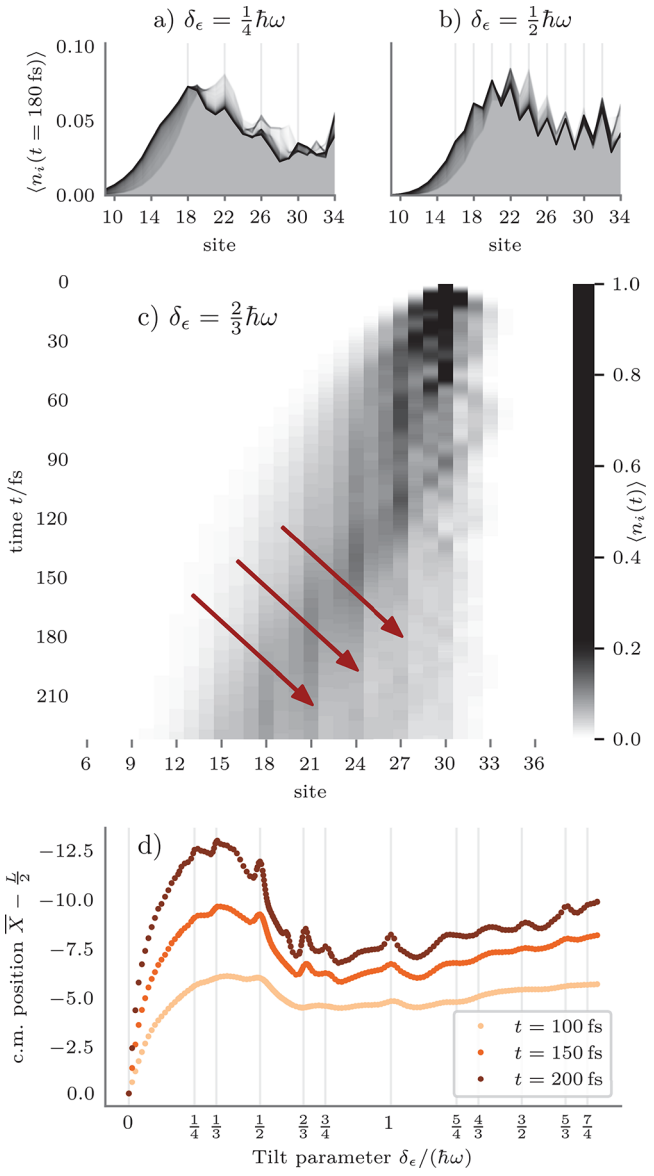

Figure 4. Resonant tunneling with parameters corresponding to the DNA-scaffolded Cy3 system demonstrated by Hart et al.[62] (a,b) The local exciton distribution 180 fs after initial excitation for two resonant energy gradients, with vertical lines as visual aids for the resonance interval, and shadows indicating the distribution over the preceding 30 fs. (c) The time evolution of the local exciton density for a 3-bond resonant tilt. Edges of resonance-induced high density are marked by arrows. (d) Center-of-mass position for a range of tilts (cf., Figure 2c,d) with simple rationals $\delta_\epsilon = m/n\hbar\omega$ up to $n = 4$ marked by vertical lines. $n = 5$ resonances are also partially discernible. The initial state is a Franck–Condon excitation from the center site [c,d] (or the last site [a,b] for clarity). Parts of the chain not shown in panels a–c for clarity. $\hbar\omega = 1150\ \mathrm{cm}^{-1}$; $J = 0.55\hbar\omega = 632.5\ \mathrm{cm}^{-1}$; $g = 0.71\hbar\omega$ ($S = 0.50$); $L = 35$ in a), b), $L = 61$ in c), d), except for $L = 75$ where $\delta_\epsilon/(\hbar\omega) \in \{0, 0.0125\}$.

The basis of the approach is to first consider a dimer, $L = 2$, and separate the total Hamiltonian H (eq 1) into the hopping operator $T = J(|0\rangle\langle 1| + |1\rangle\langle 0|)$ and $H_0 := H - T$. Then the initial state is taken to be localized to $|0\rangle$ and the time-dependent transition probability is calculated as $q(t, \delta_\epsilon) := \langle 1|U^{(1)}(t)|0\rangle$ using the first-order propagator $U^{(1)}(t)$. After tracing out the phononic degrees of freedom and evaluating the propagators using path integrals, we obtain

$$q(t, \delta_\epsilon) = \left|\frac{J}{\hbar}\right|^2 \int_0^t \mathrm{d}\tau_1 \int_0^t \mathrm{d}\tau_2 \exp\Big\{2S(\mathrm{e}^{-i\omega(\tau_1-\tau_2)} - 1) + 2iS[\sin(\omega\tau_1) - \sin(\omega\tau_2)] - i\frac{\delta_\epsilon}{\hbar}(\tau_1 - \tau_2)\Big\} \tag{2}$$

where $S = \left(\frac{g}{\hbar\omega}\right)^2$ is the Huang–Rhys factor. These transition probabilities are extended to a chain of length $L > 2$ by applying the dimer transition probability on each bond.

To explain the vibronic resonance, we examine the properties of $q(t, \delta_\epsilon)$ in eq 2. Define $F(\tau_1, \tau_2)$ as the integrand of $q(t, \delta_\epsilon)$ for $\delta_\epsilon = 0$. Then $F(\tau_1, \tau_2)$ is periodic in both arguments with a period $T = \frac{2\pi}{\omega}$. Now, for general $\delta_\epsilon \in \mathbb{R}$, we can write the transition probability in eq 2 as the 2D Fourier transform of $\chi_{[0,t]^2}F(\tau_1, \tau_2)$ evaluated at $\left(\frac{\delta_\epsilon}{\hbar}, -\frac{\delta_\epsilon}{\hbar}\right)$, where $\chi_{[0,t]^2}$ is the two-dimensional boxcar function on τ_1, τ_2. In the absence of $\chi_{[0,t]^2}$, the transfer probability $q(t, \delta_\epsilon)$ would vanish unless the Fourier frequency matches the periodicity of F:

$$\frac{\delta_\epsilon}{\hbar} = m\frac{2\pi}{T} = m\omega \quad \text{for} \quad m \in \mathbb{N}_0$$

This is the first-order vibronic resonance condition and demonstrates how the resonance peaks arise. When taking into account $\chi_{[0,t]^2}$, which acts as a 2D convolution in frequency space, and using the Dirac comb structure of $\hat{F}$, we find that

$$q(t, \delta_\epsilon)|_{\delta_\epsilon \approx m\hbar\omega} \approx 2c_m \frac{1 - \cos\left(t\left(\frac{\delta_\epsilon}{\hbar} - m\omega\right)\right)}{\left(\frac{\delta_\epsilon}{\hbar} - m\omega\right)^2} \tag{3}$$

where c_m is the Fourier coefficient of F at $\omega_1 = -\omega_2 = m\omega$. Equation 3 determines the structure of a resonance peak at $\delta_\epsilon = m\hbar\omega$ and shows the oscillatory structure of the transient side-peaks around the main resonance peaks. Furthermore, one can easily see from a Taylor expansion of the cosine that the main peaks at $\delta_\epsilon = m\hbar\omega$ become sharper and taller with $\sim t^2$. Both the oscillatory side-peaks and the quadratic growth of the main peaks are confirmed in Figure 2a).

Physically, the first-order perturbation describes the transition between adjacent sites, which differ in energy by δ_ϵ. In accord with energy conservation, the transition is allowed if the vibrational energy difference $m\hbar\omega$ matches the tilt energy, $m\hbar\omega = \delta_\epsilon$. More generally, to capture long-range tunneling over n bonds, an nth order perturbative expansion would be required, leading to the generalized fractional resonance condition $m\hbar\omega = n\delta_\epsilon$.

In Figure 2a,c, we compare the perturbative dynamics to the numerical results for $J = -\frac{1}{10}\hbar\omega$, which shows excellent agreement between the results. Both methods show first-order tunneling spikes around integer multiples of $\hbar\omega$. The weak J suppresses higher-order tunneling events and the associated spikes at rational fractions $m/n\hbar\omega$ (though *transient* side-peaks appear, predicted by eq 3). A small but persistent second-order tunneling effect is observable only in the full numerical calculations (see SI section 5). For $\delta_\epsilon \lesssim 0.1\hbar\omega$, we observe linear response behavior for short times (SI section 6).

https://doi.org/10.1021/acs.jpclett.2c01455
J. Phys. Chem. Lett. 2022, 13, 6831–6838

APPLICATION TO ENGINEERED CY3 SYSTEM

The analysis so far has clearly demonstrated our mechanism for an abstract Holstein model. To investigate its impact in realistic systems, we choose an oligomeric extension of the recently demonstrated DNA-scaffolded tunable Cy3 dyes[62,63] as a model system and numerically calculate the dynamics using the adjacent-dimer (0-nt) parameters for each nearest-neighbor interaction: $\hbar\omega$ = 1150 cm^{-1}, $J = 0.55\hbar\omega$ = 632.5 cm^{-1} (H-aggregate coupling), and $g = 0.71\hbar\omega$ (S = 0.50). Since the polaronic trapping is much weaker for this smaller Huang–Rhys factor S, the chain length is increased to L = 61 to eliminate boundary effects while ν_{max} is decreased to 15. The results of these calculations can be seen in Figure 4. We see the same resonance features at simple rational fractions $\delta_\epsilon = m/n\hbar\omega$, including more long-ranged (higher n) resonances enabled by the greater chain length. The features are clearly visible albeit less distinct than in Figure 2, as is to be expected due to the decreased dominance of the vibronic dynamics over the excitonic dynamics. This also causes Bloch[64] (or Wannier–Stark[65−67]) localization to arise, which is the reason behind the momentary *decrease* in transport as δ_ϵ increases beyond $\frac{\hbar\omega}{3}$. These results provide a proof-of-principle for a typical and realistic parameter regime, but we note that our model assumes fully coherent transport and does not include disorder, temperature, additional phonon modes or a dissipative bath, which we discuss below. Furthermore, practical aspects of the implementation of said model system would also need to be considered: If the energy gradient in our model is given by an electric field, then it may distort the HOMO–LUMO gaps or vibrational modes in unexpected ways. Alternatively, it may be achieved via chemical engineering, possibly by substitution of Cy3 with Cy5, etc. Moreover, the localized initial state may be difficult to attain via optical excitation (localized excitation via an excitation donor may be a possible alternative), but we note that the proposed resonance mechanism is not fundamentally dependent on a fully localized initial state and should carry over to partially delocalized states.

THE EFFECTS OF DISORDER, NOISE, RELAXATION, AND LONG-RANGE COUPLING

The typically large phonon energies of vibronically active modes mean that even at room temperature, the probability of finding the initial state (pre-excitation) in anything but the vibrational ground state is negligible ($e^{-\hbar\omega/k_BT} < 0.5\%$ for $\hbar\omega$ = 1150 cm^{-1}), and therefore nonzero temperatures *alone* would leave the results virtually unchanged. Meanwhile, we can expect static disorder to broaden the regular spatial structure of the tunneling peaks; however, this is not necessarily detrimental for the overall mobility, as disordered site energies may coincide with phonon energies, even over longer distances, as we show. Finally, further bath modes or "noise" may have the largest impact, as it is easy to see that including a second, equally strongly coupled mode would double the number of resonant peaks, and thus a large number of strongly coupled vibrational modes would smear out the entire signal. However, we note two points: First, even though this situation would broaden the resonance *signatures*, it does not necessarily suppress the overall *resonant mobility*, and second, many molecular systems have few or a single strongly coupled dominant vibrational mode prevailing over the other modes (ostensibly the case for the Cy3–DNA system). Apart from coupling the *exciton* to further modes, the *vibrational mode* may also be damped by further modes. Though a full treatment of this damped-vibration setup is beyond the scope of our pure-state method, we investigate approximations of such a situation in the SI section 7, where we find vibrationally relaxed initial states may increase the "downhill" directionality at the expense of overall mobility. More in-depth analyses of the effect of such dissipative terms would be the topic of further research.[68]

Furthermore, lifting the restriction of purely nearest-neighbor coupling is an important extension for realistic, dipole–dipole-coupled systems. As the crucial ingredient to our mechanism is the energetic resonance between different vibronic states, including longer-range interaction is no detriment to the resonant tunneling. In the SI section 8 we present numerical data for a version of the Cy3 model calculations that include next-to-nearest-neighbor coupling, in which the resonance peaks are in fact found to be slightly sharper than with purely nearest-neighbor coupling.

CONCLUSION AND OUTLOOK

We have uncovered resonance-dependent transport behavior in tilted vibronic chains. Tunneling over n bonds is allowed for $\delta_\epsilon/(\hbar\omega) = m/n$, corresponding to m-phonon and nth order tunneling transitions. To study this problem, we have developed both an analytical and a numerical method. We also considered robustness against temperature, disorder, and dissipation and provided an outlook on the effect of non-nearest-neighbor coupling and vibrationally relaxed states.

This generalizes the resonant tunneling found in Mott insulators on tilted Bose–Hubbard chains,[30,33,37] as long-range, repeated hopping in both directions is naturally obtained. Vibronic coherence has also emerged as an active mechanism in light-harvesting systems, molecular semiconductors, and molecular electronics. Our discovery of long-range tunneling resonances have an important bearing on the "phonon antenna" mechanism,[69,70] a new type of environment-assisted quantum transport.[71] Prospective technological applications are to exploit the bias-dependent resonance peaks for optimization or selective switching of quantum transport, or to enable nanoscale sensing of structural parameters, for example, as an extension of inelastic electron tunneling spectroscopy (cf., ref 72). Future efforts will aim at extensions from the chain configuration to thin films, nanotubes, and quantum networks, and determine the influence of coupling to further bath modes (cf., ref 73). Calculations of noisy driven energy transfer in a dimer suggest that such behavior is indeed robust.[24] Furthermore, we expect this behavior can be realized in quantum simulators using tilted optical lattices[74−76] or superconducting qubits.[77−79]

ASSOCIATED CONTENT

Supporting Information

The Supporting Information is available free of charge at https://pubs.acs.org/doi/10.1021/acs.jpclett.2c01455.

Details on the numerical method; g- and J-independence of resonance between $\hbar\omega$ and δ_ϵ; position-space profile of long-range tunneling for $\delta_\epsilon = \frac{\hbar\omega}{n}$; treatment of sign flips of J; numerically observable second-order tunneling for $J = -\hbar\omega$; linear response for small δ_ϵ; vibrationally relaxed initial states; dipole–dipole-type non-nearest-neighbor coupling (PDF)

https://doi.org/10.1021/acs.jpclett.2c01455
J. Phys. Chem. Lett. 2022, 13, 6831−6838

AUTHOR INFORMATION

Corresponding Authors

R. Kevin Kessing − *Institut für Theoretische Physik, Universität Ulm, Ulm 89069, Germany; Institut für Theoretische Physik, Georg-August-Universität Göttingen, Göttingen 37077, Germany; Department of Chemistry, Massachusetts Institute of Technology, Cambridge, Massachusetts 02139, United States;* orcid.org/0000-0001-9614-4778; Email: kevin.kessing@uni-ulm.de

Pei-Yun Yang − *Department of Physics, National Taiwan University, Taipei 10617, Taiwan (R.O.C.); Beijing Computational Science Research Center, Beijing 100193, China; Department of Chemistry, Massachusetts Institute of Technology, Cambridge, Massachusetts 02139, United States;* Email: pyyang@phys.ntu.edu.tw

Salvatore R. Manmana − *Institut für Theoretische Physik, Georg-August-Universität Göttingen, Göttingen 37077, Germany; Fachbereich Physik, Philipps-Universität Marburg, Marburg 35032, Germany*; Email: salvatore.manmana@uni-goettingen.de

Jianshu Cao − *Department of Chemistry, Massachusetts Institute of Technology, Cambridge, Massachusetts 02139, United States;* orcid.org/0000-0001-7616-7809; Email: jianshu@mit.edu

Complete contact information is available at: https://pubs.acs.org/10.1021/acs.jpclett.2c01455

Notes

The authors declare no competing financial interest.

ACKNOWLEDGMENTS

We thank Fabian Heidrich-Meisner, Martin Plenio, and Andrea Mattioni for insightful discussions and feedback, as well as Benedikt Kloss for providing access to numerical data and Gabriela Schlau-Cohen and her group for providing information on the Cy3 system. R.K.K. acknowledges generous scholarships and travel funds provided by the Studienstiftung des deutschen Volkes. P.Y.Y. acknowledges support from National Natural Science Foundation of China (Grant No. U1930402). R.K.K. and S.R.M. acknowledge funding by the Deutsche Forschungsgemeinschaft (DFG, German Research Foundation)—217133147/SFB 1073, project B03. J.C. acknowledges support from the NSF (Grants No. CHE 1800301 and No. CHE 1836913) and MIT Sloan Fund. R.K.K. acknowledges computational resources provided by the state of Baden-Württemberg through bwHPC and the DFG through Grant No. INST 40/575-1 FUGG (JUSTUS 2 cluster), and gratefully acknowledges GPU resources provided by the Institute of Theoretical Physics in Göttingen and financed by the DFG and the Bundesministerium für Bildung und Foschung (BMBF).

REFERENCES

(1) May, V.; Kühn, O. *Charge and Energy Transfer Dynamics in Molecular Systems*, Third Edition; Wiley-VCH: 2011, DOI: 10.1002/9783527633791.

(2) Coropceanu, V.; Cornil, J.; da Silva Filho, D. A.; Olivier, Y.; Silbey, R.; Brédas, J.-L. Charge Transport in Organic Semiconductors. *Chem. Rev.* **2007**, *107*, 926−952.

(3) Cheng, Y.-C.; Silbey, R. J. A Unified Theory for Charge-Carrier Transport in Organic Crystals. *J. Chem. Phys.* **2008**, *128*, 114713.

(4) Ortmann, F.; Bechstedt, F.; Hannewald, K. Theory of Charge Transport in Organic Crystals: Beyond Holstein's Small-Polaron Model. *Phys. Rev. B* **2009**, *79*, 235206.

(5) Womick, J. M.; Moran, A. M. Vibronic Enhancement of Exciton Sizes and Energy Transport in Photosynthetic Complexes. *J. Phys. Chem. B* **2011**, *115*, 1347−1356.

(6) Schröter, M.; Ivanov, S.; Schulze, J.; Polyutov, S.; Yan, Y.; Pullerits, T.; Kühn, O. Exciton−Vibrational Coupling in the Dynamics and Spectroscopy of Frenkel Excitons in Molecular Aggregates. *Phys. Rep.* **2015**, *567*, 1−78.

(7) Huang, Z.; Chen, L.; Zhou, N.; Zhao, Y. Transient Dynamics of a One-Dimensional Holstein Polaron under the Influence of an External Electric Field. *Ann. Phys. (Berlin)* **2017**, *529*, 1600367.

(8) Hestand, N. J.; Spano, F. C. Expanded Theory of H- and J-Molecular Aggregates: The Effects of Vibronic Coupling and Intermolecular Charge Transfer. *Chem. Rev.* **2018**, *118*, 7069−7163.

(9) Kundu, S.; Makri, N. Exciton−Vibration Dynamics in J-Aggregates of a Perylene Bisimide from Real-Time Path Integral Calculations. *J. Phys. Chem. C* **2021**, *125*, 201−210.

(10) Li, W.; Ren, J.; Shuai, Z. A General Charge Transport Picture for Organic Semiconductors with Nonlocal Electron−Phonon Couplings. *Nat. Commun.* **2021**, *12*, 4260.

(11) Khan, F. S.; Davies, J. H.; Wilkins, J. W. Quantum Transport Equations for High Electric Fields. *Phys. Rev. B* **1987**, *36*, 2578−2597.

(12) Rott, S.; Linder, N.; Döhler, G. H. Field Dependence of the Hopping Drift Velocity in Semiconductor Superlattices. *Phys. Rev. B* **2002**, *65*, 195301.

(13) Cao, J.; Cogdell, R. J.; Coker, D. F.; Duan, H.-G.; Hauer, J.; Kleinekathöfer, U.; Jansen, T. L. C.; Mančal, T.; Miller, R. J. D.; Ogilvie, J. P. Quantum Biology Revisited. *Sci. Adv.* **2020**, *6*, 4888.

(14) Wu, J.; Liu, F.; Shen, Y.; Cao, J.; Silbey, R. J. Efficient Energy Transfer in Light-Harvesting Systems, I: Optimal Temperature, Reorganization Energy and Spatial−Temporal Correlations. *New J. Phys.* **2010**, *12*, 105012.

(15) Roulleau, P.; Baer, S.; Choi, T.; Molitor, F.; Güttinger, J.; Müller, T.; Dröscher, S.; Ensslin, K.; Ihn, T. Coherent Electron-Phonon Coupling in Tailored Quantum Systems. *Nat. Commun.* **2011**, *2*, 239.

(16) Goldberg, O.; Meir, Y.; Dubi, Y. Vibration-Assisted and Vibration-Hampered Excitonic Quantum Transport. *J. Phys. Chem. Lett.* **2018**, *9*, 3143−3148.

(17) Cui, Y.; Tosoni, S.; Schneider, W.-D.; Pacchioni, G.; Nilius, N.; Freund, H.-J. Phonon-Mediated Electron Transport through CaO Thin Films. *Phys. Rev. Lett.* **2015**, *114*, 016804.

(18) Jung, S.; Park, M.; Park, J.; Jeong, T.-Y.; Kim, H.-J.; Watanabe, K.; Taniguchi, T.; Ha, D. H.; Hwang, C.; Kim, Y.-S. Vibrational Properties of h-BN and h-BN-Graphene Heterostructures Probed by Inelastic Electron Tunneling Spectroscopy. *Sci. Rep.* **2015**, *5*, 16642.

(19) Vdovin, E. E.; Mishchenko, A.; Greenaway, M. T.; Zhu, M. J.; Ghazaryan, D.; Misra, A.; Cao, Y.; Morozov, S. V.; Makarovsky, O.; Fromhold, T. M.; et al. Phonon-Assisted Resonant Tunneling of Electrons in Graphene-Boron Nitride Transistors. *Phys. Rev. Lett.* **2016**, *116*, 186603.

(20) Koch, J.; von Oppen, F. Franck-Condon Blockade and Giant Fano Factors in Transport through Single Molecules. *Phys. Rev. Lett.* **2005**, *94*, 206804.

(21) Leturcq, R.; Stampfer, C.; Inderbitzin, K.; Durrer, L.; Hierold, C.; Mariani, E.; Schultz, M. G.; von Oppen, F.; Ensslin, K. Franck−Condon Blockade in Suspended Carbon Nanotube Quantum Dots. *Nat. Phys.* **2009**, *5*, 327−331.

(22) Kolli, A.; O'Reilly, E. J.; Scholes, G. D.; Olaya-Castro, A. The Fundamental Role of Quantized Vibrations in Coherent Light Harvesting by Cryptophyte Algae. *J. Chem. Phys.* **2012**, *137*, 174109.

(23) Tiwari, V.; Peters, W. K.; Jonas, D. M. Electronic Resonance with Anticorrelated Pigment Vibrations Drives Photosynthetic Energy Transfer outside the Adiabatic Framework. *Proc. Natl. Acad. Sci. U.S.A.* **2013**, *110*, 1203−1208.

(24) Dijkstra, A. G.; Wang, C.; Cao, J.; Fleming, G. R. Coherent Exciton Dynamics in the Presence of Underdamped Vibrations. *J. Phys. Chem. Lett.* **2015**, *6*, 627−632.
(25) Maekawa, S. Nonlinear Conduction of ZnS in Strong Electric Fields. *Phys. Rev. Lett.* **1970**, *24*, 1175−1177.
(26) Kümmel, R.; Rauh, H.; Bangert, E. Theory of Stark-Ladder Currents. *Phys. Status Solidi B* **1978**, *87*, 99−110.
(27) Moix, J. M.; Khasin, M.; Cao, J. Coherent Quantum Transport in Disordered Systems: I. The Influence of Dephasing on the Transport Properties and Absorption Spectra on One-Dimensional Systems. *New J. Phys.* **2013**, *15*, 085010.
(28) Emin, D.; Hart, C. F. Phonon-Assisted Hopping of an Electron on a Wannier-Stark Ladder in a Strong Electric Field. *Phys. Rev. B* **1987**, *36*, 2530−2546.
(29) Vidmar, L.; Bonča, J.; Mierzejewski, M.; Prelovšek, P.; Trugman, S. A. Nonequilibrium Dynamics of the Holstein Polaron Driven by an External Electric Field. *Phys. Rev. B* **2011**, *83*, 134301.
(30) Sachdev, S.; Sengupta, K.; Girvin, S. M. Mott Insulators in Strong Electric Fields. *Phys. Rev. B* **2002**, *66*, 075128.
(31) Sias, C.; Zenesini, A.; Lignier, H.; Wimberger, S.; Ciampini, D.; Morsch, O.; Arimondo, E. Resonantly Enhanced Tunneling of Bose−Einstein Condensates in Periodic Potentials. *Phys. Rev. Lett.* **2007**, *98*, 120403.
(32) Pielawa, S.; Kitagawa, T.; Berg, E.; Sachdev, S. Correlated Phases of Bosons in Tilted Frustrated Lattices. *Phys. Rev. B* **2011**, *83*, 205135.
(33) Simon, J.; Bakr, W. S.; Ma, R.; Tai, M. E.; Preiss, P. M.; Greiner, M. Quantum Simulation of Antiferromagnetic Spin Chains in an Optical Lattice. *Nature* **2011**, *472*, 307−312.
(34) Rubbo, C. P.; Manmana, S. R.; Peden, B. M.; Holland, M. J.; Rey, A. M. Resonantly Enhanced Tunneling and Transport of Ultracold Atoms on Tilted Optical Lattices. *Phys. Rev. A* **2011**, *84*, 033638.
(35) Carrasquilla, J.; Manmana, S. R.; Rigol, M. Scaling of the Gap, Fidelity Susceptibility, and Bloch Oscillations Across the Superfluid-to-Mott-Insulator Transition in the One-Dimensional Bose-Hubbard Model. *Phys. Rev. A* **2013**, *87*, 043606.
(36) Meinert, F.; Mark, M. J.; Kirilov, E.; Lauber, K.; Weinmann, P.; Daley, A. J.; Nägerl, H.-C. Quantum Quench in an Atomic One-Dimensional Ising Chain. *Phys. Rev. Lett.* **2013**, *111*, 053003.
(37) Meinert, F.; Mark, M. J.; Kirilov, E.; Lauber, K.; Weinmann, P.; Gröbner, M.; Daley, A. J.; Nägerl, H.-C. Observation of Many-Body Dynamics in Long-Range Tunneling after a Quantum Quench. *Science* **2014**, *344*, 1259−1262.
(38) Buyskikh, A. S.; Tagliacozzo, L.; Schuricht, D.; Hooley, C. A.; Pekker, D.; Daley, A. J. Spin Models, Dynamics, and Criticality with Atoms in Tilted Optical Superlattices. *Phys. Rev. Lett.* **2019**, *123*, 090401.
(39) Buyskikh, A. S.; Tagliacozzo, L.; Schuricht, D.; Hooley, C. A.; Pekker, D.; Daley, A. J. Resonant Two-Site Tunneling Dynamics of Bosons in a Tilted Optical Superlattice. *Phys. Rev. A* **2019**, *100*, 023627.
(40) Gorshkov, A. V.; Manmana, S. R.; Chen, G.; Ye, J.; Demler, E.; Lukin, M. D.; Rey, A. M. Tunable Superfluidity and Quantum Magnetism with Ultracold Polar Molecules. *Phys. Rev. Lett.* **2011**, *107*, 115301.
(41) Keilmann, T.; Lanzmich, S.; McCulloch, I.; Roncaglia, M. Statistically Induced Phase Transitions and Anyons in 1D Optical Lattices. *Nat. Commun.* **2011**, *2*, 361.
(42) Kloss, B.; Reichman, D. R.; Tempelaar, R. Multiset Matrix Product State Calculations Reveal Mobile Franck-Condon Excitations under Strong Holstein-Type Coupling. *Phys. Rev. Lett.* **2019**, *123*, 126601.
(43) Shalashilin, D. V.; Child, M. S. Time Dependent Quantum Propagation in Phase Space. *J. Chem. Phys.* **2000**, *113*, 10028−10036.
(44) Shalashilin, D. V.; Child, M. S. Real Time Quantum Propagation on a Monte Carlo Trajectory Guided Grids of Coupled Coherent States: 26D Simulation of Pyrazine Absorption Spectrum. *J. Chem. Phys.* **2004**, *121*, 3563−3568.
(45) Ben-Nun, M.; Quenneville, J.; Martínez, T. J. Ab Initio Multiple Spawning: Photochemistry from First Principles Quantum Molecular Dynamics. *J. Phys. Chem. A* **2000**, *104*, 5161−5175.
(46) Gu, B.; Garashchuk, S. Quantum Dynamics with Gaussian Bases Defined by the Quantum Trajectories. *J. Phys. Chem. A* **2016**, *120*, 3023−3031.
(47) Werther, M.; Großmann, F. Apoptosis of Moving Non-orthogonal Basis Functions in Many-Particle Quantum Dynamics. *Phys. Rev. B* **2020**, *101*, 174315.
(48) Koch, W.; Frankcombe, T. J. Basis Expansion Leaping: ANew Method to Solve the Time-Dependent Schrödinger Equation for Molecular Quantum Dynamics. *Phys. Rev. Lett.* **2013**, *110*, 263202.
(49) Richings, G.; Polyak, I.; Spinlove, K.; Worth, G.; Burghardt, I.; Lasorne, B. Quantum Dynamics Simulations Using Gaussian Wavepackets: the vMCG Method. *Int. Rev. Phys. Chem.* **2015**, *34*, 269−308.
(50) Saller, M. A. C.; Habershon, S. Quantum Dynamics with Short-Time Trajectories and Minimal Adaptive Basis Sets. *J. Chem. Theory Comput.* **2017**, *13*, 3085−3096.
(51) Hartke, B. Propagation with Distributed Gaussians as a Sparse, Adaptive Basis for Higher-Dimensional Quantum Dynamics. *Phys. Chem. Chem. Phys.* **2006**, *8*, 3627−3635.
(52) Sielk, J.; von Horsten, H. F.; Krüger, F.; Schneider, R.; Hartke, B. Quantum-Mechanical Wavepacket Propagation in a Sparse, Adaptive Basis of Interpolating Gaussians with Collocation. *Phys. Chem. Chem. Phys.* **2009**, *11*, 463−475.
(53) Bonča, J.; Trugman, S. A.; Batistić, I. Holstein Polaron. *Phys. Rev. B* **1999**, *60*, 1633−1642.
(54) Dorfner, F.; Vidmar, L.; Brockt, C.; Jeckelmann, E.; Heidrich-Meisner, F. Real-Time Decay of a Highly Excited Charge Carrier in the One-Dimensional Holstein Model. *Phys. Rev. B* **2015**, *91*, 104302.
(55) Bonča, J.; Trugman, S. A. Inelastic Quantum Transport. *Phys. Rev. Lett.* **1997**, *79*, 4874−4877.
(56) Glauber, R. J. Coherent and Incoherent States of the Radiation Field. *Phys. Rev.* **1963**, *131*, 2766−2788.
(57) Cao, J.; Silbey, R. J. Optimization of Exciton Trapping in Energy Transfer Processes. *J. Phys. Chem. A* **2009**, *113*, 13825−13838.
(58) Wu, J.; Cao, J. Higher-Order Kinetic Expansion of Quantum Dissipative Dynamics: Mapping Quantum Networks to Kinetic Networks. *J. Chem. Phys.* **2013**, *139*, 044102.
(59) Cerrillo, J.; Cao, J. Non-Markovian Dynamical Maps: Numerical Processing of Open Quantum Trajectories. *Phys. Rev. Lett.* **2014**, *112*, 110401.
(60) Shlesinger, M. F. Asymptotic Solutions of Continuous-Time Random Walks. *J. Stat. Phys.* **1974**, *10*, 421−434.
(61) Witkoskie, J. B.; Cao, J. Aging Correlation Functions of the Interrupted Fractional Fokker-Planck Propagator. *J. Chem. Phys.* **2006**, *125*, 244511.
(62) Hart, S. M.; Chen, W. J.; Banal, J. L.; Bricker, W. P.; Dodin, A.; Markova, L.; Vyborna, Y.; Willard, A. P.; Häner, R.; Bathe, M.; et al. Engineering Couplings for Exciton Transport Using Synthetic DNA Scaffolds. *Chem.* **2021**, *7*, 752−773.
(63) Hart, S. M.; Wang, X.; Guo, J.; Bathe, M.; Schlau-Cohen, G. S. Tuning Optical Absorption and Emission Using Strongly Coupled Dimers in Programmable DNA Scaffolds. *J. Phys. Chem. Lett.* **2022**, *13*, 1863−1871.
(64) van Nieuwenburg, E.; Baum, Y.; Refael, G. From Bloch Oscillations to Many-Body Localization in Clean Interacting Systems. *Proc. Natl. Acad. Sci. U.S.A.* **2019**, *116*, 9269−9274.
(65) Bleuse, J.; Bastard, G.; Voisin, P. Electric-Field-Induced Localization and Oscillatory Electro-Optical Properties of Semiconductor Superlattices. *Phys. Rev. Lett.* **1988**, *60*, 220−223.
(66) Mendez, E. E.; Agulló-Rueda, F.; Hong, J. M. Stark Localization in GaAs-GaAlAs Superlattices under an Electric Field. *Phys. Rev. Lett.* **1988**, *60*, 2426−2429.
(67) Weiser, G.; Weihofen, R.; Perales, A.; Starck, C. Stark Effect and Wannier-Stark Localization in InGaAs Quantum Wells. LEOS 1992 Summer Topical Meeting Digest on Broadband Analog and Digital Optoelectronics, Optical Multiple Access Networks, Integrated

https://doi.org/10.1021/acs.jpclett.2c01455
J. Phys. Chem. Lett. 2022, 13, 6831−6838

Optoelectronics, and Smart Pixels, Santa Barbara, California, July 29–August 12, 1992; pp 580–583.
(68) Lee, C. K.; Moix, J.; Cao, J. Coherent Quantum Transport in Disordered Systems: A Unified Polaron Treatment of Hopping and Band-Like Transport. *J. Chem. Phys.* **2015**, *142*, 164103.
(69) Chin, A. W.; Huelga, S. F.; Plenio, M. B. Coherence and Decoherence in Biological Systems: Principles of Noise-Assisted Transport and the Origin of Long-Lived Coherences. *Philos. Trans. R. Soc. A* **2012**, *370*, 3638–3657.
(70) Rey, M. d.; Chin, A. W.; Huelga, S. F.; Plenio, M. B. Exploiting Structured Environments for Efficient Energy Transfer: The Phonon Antenna Mechanism. *J. Phys. Chem. Lett.* **2013**, *4*, 903–907.
(71) Mohseni, M., Omar, Y., Engel, G. S., Plenio, M. B., Eds. *Quantum Effects in Biology*; Cambridge University Press, 2014.
(72) Galperin, M.; Ratner, M. A.; Nitzan, A. Molecular Transport Junctions: Vibrational Effects. *J. Phys.: Condens. Matter* **2007**, *19*, 103201.
(73) Chuang, C.; Lee, C. K.; Moix, J. M.; Knoester, J.; Cao, J. Quantum Diffusion on Molecular Tubes: Universal Scaling of the 1D to 2D Transition. *Phys. Rev. Lett.* **2016**, *116*, 196803.
(74) Pazy, E.; Vardi, A. Holstein Model and Peierls Instability in One-Dimensional Boson-Fermion Lattice Gases. *Phys. Rev. A* **2005**, *72*, 033609.
(75) Schäfer, F.; Fukuhara, T.; Sugawa, S.; Takasu, Y.; Takahashi, Y. Tools for Quantum Simulation with Ultracold Atoms in Optical Lattices. *Nat. Rev. Phys.* **2020**, *2*, 411–425.
(76) Herrera, F.; Krems, R. V. Tunable Holstein Model with Cold Polar Molecules. *Phys. Rev. A* **2011**, *84*, 051401.
(77) Mostame, S.; Rebentrost, P.; Eisfeld, A.; Kerman, A. J.; Tsomokos, D. I.; Aspuru-Guzik, A. Quantum Simulator of an Open Quantum System Using Superconducting Qubits: Exciton Transport in Photosynthetic Complexes. *New J. Phys.* **2012**, *14*, 105013.
(78) Potočnik, A.; Bargerbos, A.; Schröder, F. A. Y. N.; Khan, S. A.; Collodo, M. C.; Gasparinetti, S.; Salathé, Y.; Creatore, C.; Eichler, C.; Türeci, H. E.; et al. Studying Light-Harvesting Models with Superconducting Circuits. *Nat. Commun.* **2018**, *9*, 904.
(79) Wang, C. S.; Curtis, J. C.; Lester, B. J.; Zhang, Y.; Gao, Y. Y.; Freeze, J.; Batista, V. S.; Vaccaro, P. H.; Chuang, I. L.; Frunzio, L.; et al. Efficient Multiphoton Sampling of Molecular Vibronic Spectra on a Superconducting Bosonic Processor. *Phys. Rev. X* **2020**, *10*, 021060.

https://doi.org/10.1021/acs.jpclett.2c01455
J. Phys. Chem. Lett. 2022, 13, 6831–6838